- 1 Title: Examination of wind speeds in sparse suburban terrain
- 2 Author names:
- 3 Amanda Worthy¹, Shuoqi Wang¹, Johnny Estephan², Peter Irwin², Arindam Chowdhury², Greg
- 4 Lyman³ and Dorothy Reed^{1,4}
- 5 Affiliations of authors:
- 6 ¹ University of Washington, Seattle WA 98195
- ⁷ Florida International University, Miami FL 33199
- 8 ³ Central Washington University, Ellensburg WA 98926
- 9 ⁴ Corresponding author: reed@uw.edu
- 10 Abstract
- Wind speeds are investigated through an analysis of field measurements on a low-rise building
- on the Central Washington University (CWU) campus in a sparse suburban terrain in Ellensburg,
- Washington. Two roof-mounted R.M. Young ultrasonic anemometers were employed in the data
- 14 collection project: one located at 21.9 m [72 ft] above ground, and the other, closer to a pedestal-
- mounted photovoltaic (PV) array at 12.5 m [41 ft] above ground. Power spectral results were
- determined, which exposed a difference in the higher frequency content. Corresponding integral
- scales of turbulence ${}^{x}L_{u}$ and turbulence intensity I_{u} values were estimated and best fit by
- Gaussian distributions. Although the wind speed data were initially collected to be used in
- 19 estimating the *net* C_p values for the panels, they provided an opportunity to examine time-
- 20 averaged wind speeds from one duration to another, i.e., the gust factor G_U . For averaging times

- from one to ten seconds, G_U displays a wide scatter, which may have implications for structural
- 22 gust response factor determination.
- 23 <u>Keywords:</u> wind engineering, field measurements, wind speed, turbulence intensity, integral
- scale of turbulence, wind spectrum, gust factor, ultrasonic anemometer

1. Introduction

25

- Wind speed time series data were collected as part of an ongoing project to characterize wind
- 27 loadings and structural behavior of full-scale in situ rooftop pedestal-mounted photovoltaic (PV)
- panels [1, 2]. Estimation of the wind pressure loadings for the PV panels requires knowledge of
- 29 the corresponding wind speeds. Wind tunnel modeling of the pressure loadings requires detailed
- 30 representation of the corresponding wind velocity spectrum. This paper examines the statistical
- 31 parameters and spectral characteristics of full-scale in situ time series records for two ultrasonic
- 32 anemometers to assess the influence of the sparse suburban terrain and the influence of the
- 33 rooftop features for the lower anemometer. The statistical parameters include the turbulence
- intensity, the integral scale of turbulence, the gust factor, and the gust response factor.
- 35 Probability distributions are fit to all parameters. The data are used to provide insight into the
- separation of wind flows at the top of the building for the lower anemometer located closer to the
- 37 PV array. It is noted that distinct differences in the high frequency region of the wind spectra at
- 38 the two anemometer locations are apparent.

2. Materials and methods

40 2.1 Data collection

- In 2021, time series wind speed data were collected as part of a collaborative effort amongst
- 42 Florida International University (FIU), Central Washington University (CWU), and the
- 43 University of Washington (UW) to investigate the modeling of full-scale wind pressure loadings

on pedestal-mounted rooftop photovoltaic (PV) arrays. The instrumented low-rise building,

Hogue Hall, is located on the CWU campus in Ellensburg, Washington. Hogue Hall is

rectangular with nominal dimensions of 12 m [40 ft] height, 42 m [138 ft] width, and 56 m [184

ft] length with a rooftop parapet wall height of 825 mm [2.7 ft]. The campus surroundings are

low-rise buildings, tennis courts, and parking lots. The terrain is assumed to be sparse suburban.

49 An aerial view of Hogue Hall is provided in Figure 1.

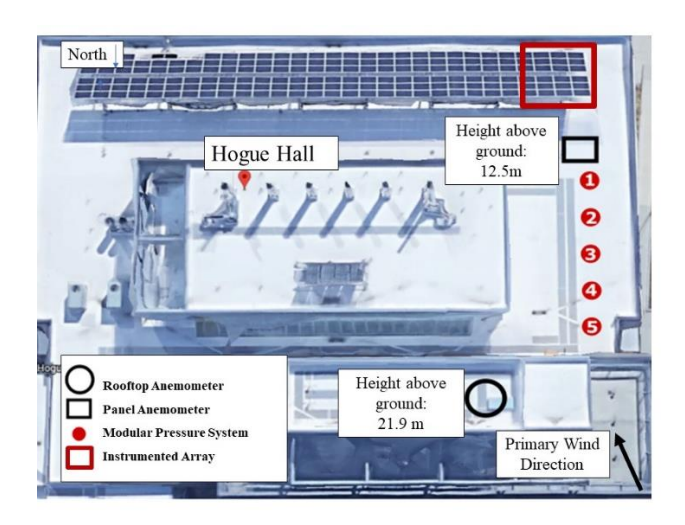


Figure 1. Aerial view of the Hogue Hall rooftop with array, pressure sensors and anemometers identified. [Source: Google Earth].

The focus in this paper is the wind speed measurements recorded by the two R.M. Young ultrasonic anemometers, models 85000 and 86000, at 21.9 m [72 ft] and 12.5 m [41 ft], respectively, identified in Figure 1. They are labeled in this paper as "rooftop" and "panel" anemometers, because the lower one was installed in front of the panel array to capture the wind speeds closer in location to the panels. It is assumed that this anemometer would have been in the disturbed shear flow created by the building itself. The rooftop anemometer was placed on a 2.82 m [9 ft 3 in] tripod on the roof on the front or north side of the building. Metal ties secured the tripod. Data were collected at the maximum recording frequency of 122 Hz for the rooftop, and 25 Hz for the panel anemometer.

The collected wind data time series were provided to LabVIEW. The data collection is set to start after 120 seconds of consistent wind speed over 4.46 m/s [10 mph] and stops after 120 seconds of consistent wind under 4.46 m/s [10 mph]. Data acquisition and storage are through National Instruments cRIO controllers. The purpose of the Real-Time Controllers is to acquire and store data remotely on-site, without the need to be directly connected to a primary computer. The controllers are connected to the primary computer via the LAN network. This allows the user to remotely modify and observe the real-time program on the controller and to remotely download the data collected after a test without having to physically retrieve the controllers' 70 flash drives. Each controller has various data acquisition modules installed to which the sensors are connected. In the next section, parameters used for data analysis are defined.

2.2 Data Analysis

62

63

64

65

66

67

68

69

71

72

76

77

78

79

80

81

73 The turbulence intensity I_u is defined as the ratio of the standard deviation to the mean wind 74 speed:

75
$$I_u = \frac{\sigma_u}{\overline{U}}$$
 where σ_u is the standard deviation and \overline{U} is the mean.

This parameter provides a measure of the size of the velocity fluctuations relative to the mean wind speed. Another important statistical parameter is the gust factor G_U . In practice, it is important to be able to convert wind speeds from a short time duration to a longer one, such as the conversion from a three-second gust U_3 to an hourly value U_{hourly} or vice-versa. The ratio of the wind speed U_t averaged over t seconds to that over 3600 seconds or an hour is defined as the gust factor G_U :

82
$$G_{U} = \frac{U_{t}}{U_{\text{hourly}}} = \frac{U_{t[\text{sec}]}}{U_{3600}}.$$
 Equation 2

Typically, these types of conversions are undertaken using the Durst formulation for gust factors [3, 4]. However, the Durst model is limited to open terrain conditions. Investigations for other terrain conditions have been undertaken in recent years e.g., [5-9]. Wieringa [5] examined gust factors over a lake and at the edge of a town. The gust factor was found to be related to surface roughness and height above ground. Ashcroft [9] investigated the influence of terrain roughness and mean wind speed on the gust factor. He found that the gust ratio is influenced by the terrain roughness but did not report a general pattern of change for ratios and the increasing wind speed. ESDU [7] investigated the variation of mean-hourly wind speeds for various terrain conditions and their influence on gust factors. Krayer and Marshall [9] examined gust factors for hurricane records and reported that an upward adjustment from the existing Durst gust values was appropriate. They also concluded that closer examination of the probability distribution function of the gust factors was in order. Schroeder and Smith [10] evaluated wind flow characteristics for Hurricane Bonnie. Their results agreed with Krayer and Marshall. They observed greater energy in the low frequency region of the longitudinal power spectrum than predicted in analytical models, and corresponding discrepancies in the estimation of integral scales. Masters [11] examined gust factors for tropical cyclone data and his results supported the Krayer-Marshall models; that is, they were larger than the Durst values. Yu and Chowdhury [12] examined gust factors for the Florida Coastal Monitoring Program (FCMP) tropical cyclone data compared with Automated Surface Observing System (ASOS) data for extratropical storms. Consistent with Krayer and Marshall, the hurricane gust factors were higher. It was also shown that the turbulence intensities increased with terrain roughness. They suggested a study of thermal stratification to assess the influence of temperature on the gusts. Empirical relationships for gust factors for various terrain conditions based upon the log law description for wind speed

83

84

85

86

87

88

89

90

91

92

93

94

95

96

97

98

99

100

101

102

103

104

- have been established [13]. One of the aims of this paper is to compare these empirical
- predictions with the in situ data. Reference [14] introduced a formulation for modifying the
- Durst equation for other terrains and hurricane wind speeds using the logarithmic law with
- 109 correction factors. The equation for G_U is as follows:

110
$$G_U = \frac{U_t(z)}{U_{mean}(z)} = 1 + \frac{\eta(z_0)c(t)}{2.5\ln\left(\frac{z}{z_0}\right)}$$
 Equation 3

- where $\eta(z_0)$ is a factor for surface roughness and c(t) is a factor for averaging time.
- ESDU 83045 [7] makes use of a peak factor g, the mean velocity U, and the turbulence
- intensity I_u as follows, in its definition of the gust factor:

114
$$G_U[aka K_{\tau}] = \frac{\hat{U}(t, T_0)}{U} = \frac{U(t, T_0) + \hat{u}(t, T_0)}{U} = 1 + gI_u$$
. Equation 4

- 115 While the peak factor g can be estimated from measured data, the ESDU document has formulated
- a methodology for estimating the second term in Equation 4 based on different gust averaging
- times (t). The following equations apply in this formulation:

118
$$g = \frac{\hat{u}(t, T_0)}{\sigma_u(t, T_0)} * \frac{\sigma_u(t, T_0)}{\sigma_u}$$
 Equation 5

119
$$\frac{\hat{u}(t,T_0)}{\sigma_u(t,T_0)} = \sqrt{2\ln\left[T_0\nu(t,T_0)\right]} + \frac{0.577}{\sqrt{2\ln\left[T_0\nu(t,T_0)\right]}}$$
 Equation 6

$$T_{\nu} = 3.13z^{0.2} \text{ seconds}$$
 Equation 7

121
$$\frac{\sigma_u(t, T_0 = 1 \text{ hour})}{\sigma_u} = 1 - 0.193 \left[\frac{T_u}{t} + 0.1 \right]^{-0.68}$$
 Equation 8

122
$$v(t, T_0 = 1 \text{ hour}) = \frac{0.007 + 0.213 {\binom{T_u}{t}}^{0.654}}{T_u}$$
 Equation 9

where T_u = the integral time scale; z = height above ground; t = gust averaging time; \hat{u} = peak value.

conjunction with the aerodynamic admittance function. The *gust factor* is part of the ASCE7 formulation of the gust *response* factor for buildings, which separates the low and high frequency contributions of the wind speed spectrum to the corresponding pressure loadings. As

Liu et al. [15] examined the ASCE7 gust effect or response factor for rigid buildings in

the low frequency region is not well understood, it was suggested that the Standard would benefit

129 from further investigation into the wind *spectrum*.

spectrum S_u at height z above ground is e.g., [14]

124

133

Various formulations for wind spectra exist in the literature e.g. [14]. Although ESDU 74030 and 74031 [16, 17] use the von Karman expression to characterize wind velocities, it has been found that the Kaimal expression is more appropriate e.g.[13]. The Kaimal expression for the

 $\frac{nS_u(z,n)}{u_*^2} = \frac{200 f}{(1+50 f)^{\frac{3}{3}}}$ Equation 10

where $f = \frac{nz}{\overline{U}(z)}$; n is frequency in Hz; $\overline{U}(z,n)$ is the mean wind speed; u_* is the friction velocity.

The integral scale of turbulence ${}^{x}L_{u}$ is defined as the integration of the autocovariance

function R_u as follows e.g.[14]

$$^{x}L_{u} = \overline{U} \int_{0}^{\infty} \frac{R_{u}(\tau)}{\sigma_{u}^{2}} d\tau = \overline{U} \int_{0}^{\infty} \rho_{u}(\tau) d\tau$$

where $R_u(\tau)$ is the autocovariance function; $\rho_u(\tau)$ is the autocorrelation; Equation 11 τ is the time lag.

Because the autocovariance R_u is the Fourier transform of the spectrum S_u , the following

equation is typically used to estimate ${}^{x}L_{u}$ e.g. [14]

$$140 {}^{x}L_{u} = \frac{\overline{U}S_{u}(n \cong 0)}{4\sigma_{u}^{2}}.$$
 Equation 12

Equation 12 implies that knowledge of the lower frequency region is critical for estimating the integral scale of turbulence.

- The method attributed to Davenport and Solari, e.g. [18-20], for estimating the influence
- of the wind spectrum on the gust factor and loading of structures, has been defined by the
- following set of equations e.g.,[15]:

$$146 G_U = 1 + g_u I_u \sqrt{P_0} Equation 13$$

$$g_u \cong \left\{ 1.175 + 2\ln\left[\tilde{t}\sqrt{\frac{P_1}{P_0}}\right] \right\}^{\frac{1}{2}}$$
 Equation 14

$$P_0 = \int_0^\infty \frac{S_u(n)}{\sigma_u^2} X(n, \tau) dn$$
 Equation 15

$$X(n,\bar{\tau}) = \frac{\sin^2\left(\pi n\bar{\tau}\right)}{\left(\pi n\bar{\tau}\right)^2}$$
 Equation 16

150
$$P_{1} = \int_{0}^{\infty} \left[\frac{n^{x} L_{u}}{\overline{U}} \right]^{2} \frac{S_{u}(n)}{\sigma_{u}^{2}} X(n, \overline{\tau}) dn$$
 Equation 17

151
$$\tilde{t} = \frac{T\overline{U}}{{}^{x}L_{u}}$$
 Equation 18

where $g_u = \text{peak factor}$; $I_u = \text{turbulence intensity}$; n = frequency in Hz; $L_u = \text{integral scale of turbulence}$;

- 152 $S_u = \text{wind speed spectrum}; \ \sigma_u^2 = \text{variance of wind speed}; \ \overline{U} = \text{mean wind speed};$ $T = \text{time duration over which the wind speed is averaged}; \ \overline{\tau} = \text{the averaging time of the peak gust.}$
- As a peak value, G_U can be fitted by an extreme value distribution. The equation for the
- probability density function y associated with the generalized extreme value distribution for x is

155
$$y = f(x \mid k, \mu, \sigma) = \left(\frac{1}{\sigma}\right) \exp\left(-\left(1 + k\frac{(x - \mu)}{\sigma}\right)^{-\frac{1}{k}}\right) \left(1 + k\frac{(x - \mu)}{\sigma}\right)^{-1 - \frac{1}{k}}$$
 Equation 19

where k, μ and σ are parameters of the distribution [21].

3. Results and Discussion

3.1 Data processing

Measurements during the windy period yielded approximately 94 one-hour time series records. The rooftop anemometer recorded slightly more data than the panel because the mean wind speed surpassed the set point of 4.46 m/s more often. Each one-hour record for the wind speed data consisted of approximately 90,000 (panel) to 440,000 (roof) observations. The directionality of the data was checked to see if there were large deviations in wind direction through wind roses. The wind roses were fitted to mean wind directions for the records. The site exhibits a strong directionality in the NW quadrant with the angles being between 315-340 degrees as shown in the wind rose of Figure 2; therefore, using each one-hour record for its entirety was considered appropriate.

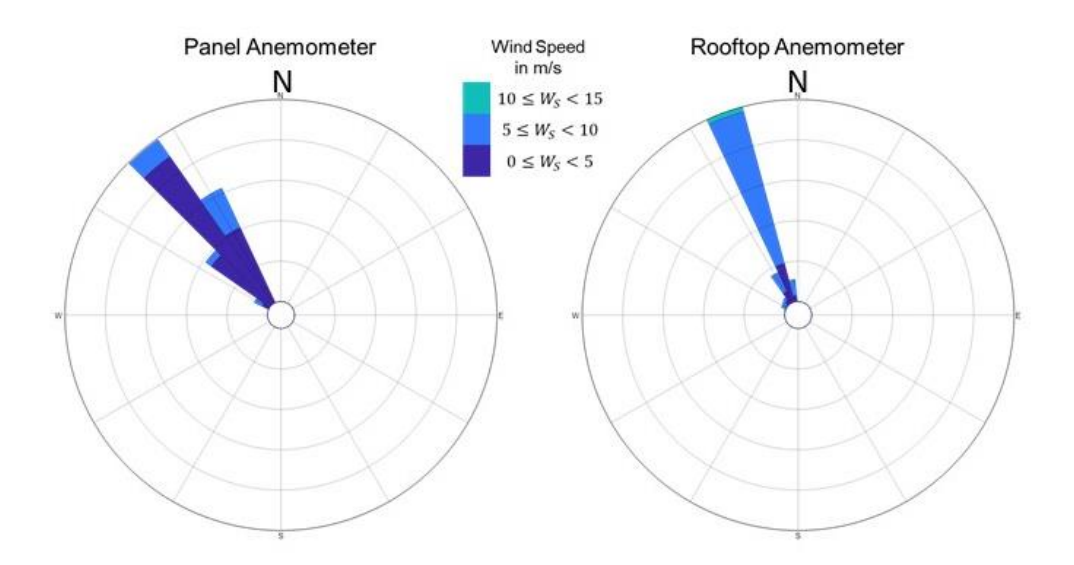


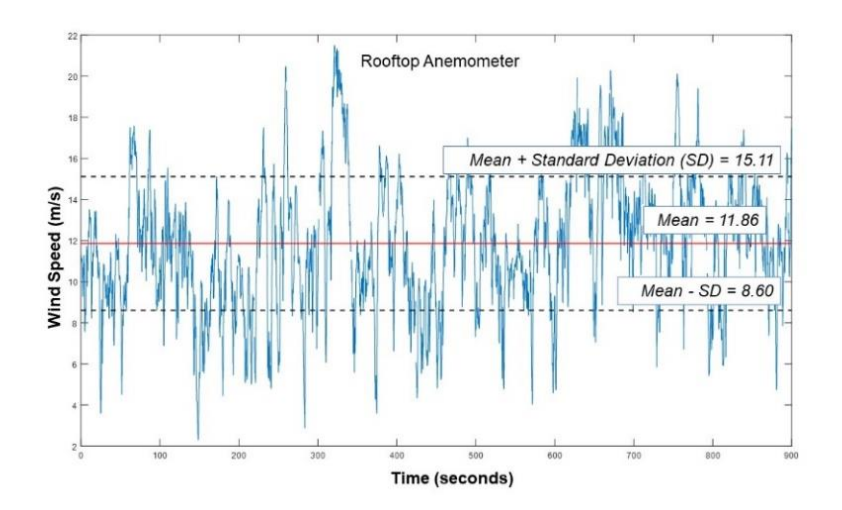
Figure 2. Wind roses for the anemometer data.

Stationarity tests were undertaken for the hour-long records. Visual inspection of the hour-long records showed storms with small or no changes to the mean value. That is, when fitting a linear regression model to the mean as a function of time, the slope was close to zero. The

substantial number of observations proved somewhat problematic for stationarity testing. That is, tabulated values are provided for observations much smaller than 90,000. The Augmented Dickey Fuller test was used on hour-long storms with the highest mean values. For these records, the *p-value* was 0.045 (< 0.05) with a test statistic of -1.986 and a critical value of -1.942 for a significance level of 5%. Hence, the Augmented Dickey Fuller test confirmed *weak* stationarity for the records. In order to compare results with previous investigations, the hourly data sets were initially separated into subsets of over four hundred 15-minute (900 seconds) packets. These data sets are examined in the next section.

3.2 Measured wind flow characteristics

An example of the wind velocity time series data is given in Figure 3 for the 15-minute highest wind speed data for the rooftop and panel data, respectively.



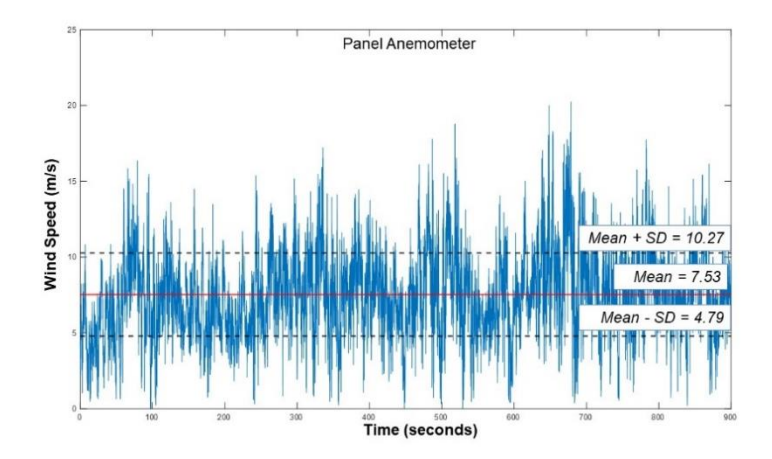


Figure 3. Rooftop and panel wind speed time series [m/s] for the highest wind speed recorded.

Figure 4 shows the corresponding spectra for the time series. The Kaimal spectrum of Equation 10 fitted to the rooftop data is shown for comparison. The rooftop data have markedly higher energy in the lower frequencies and lesser in the higher frequencies, whereas the panel record appears to have significant energy contributions for a larger range of frequencies. The slope for the rooftop spectrum is -1.8 in the higher frequency region as opposed to -1.5 (Kaimal slope).

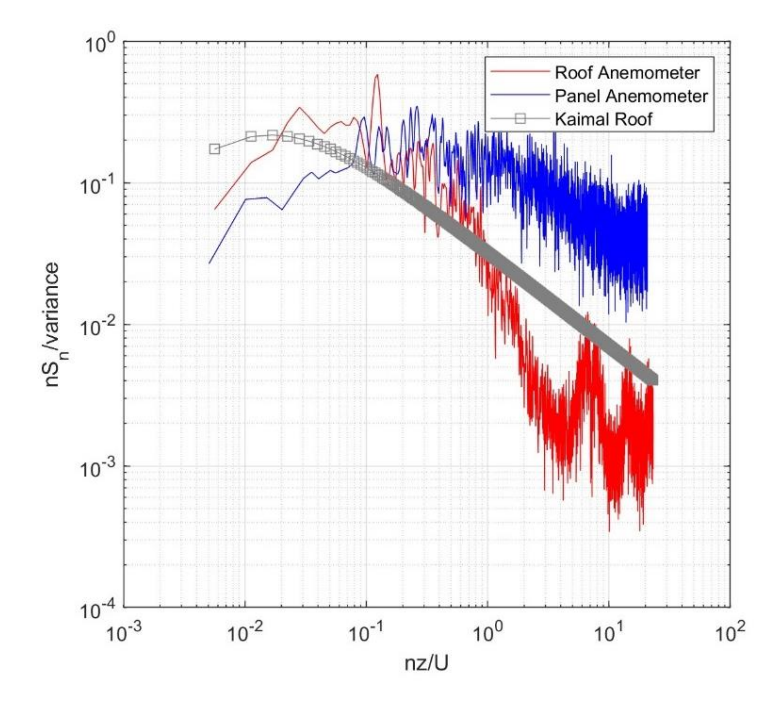


Figure 4. Sample spectra for the time series in Figure 3 normalized by the variance.

Figure 5 shows the histograms for the mean and maximum wind speeds, as well as the turbulence intensity data for the rooftop and panel. The mean hourly wind speed values ranged from 2 to 7 m/s for the panel and 3 to 12 m/s for the rooftop anemometer. The turbulence intensity I_u , defined in Equation 1 was in the range of 0.15 to 0.53, with the panel anemometer showing higher values. The panel intensities illustrate the disturbance of the wind flow near the panel array in situ. The maximum hourly wind speeds were in the range of 5 to 23 m/s. Using the log law as well as ESDU 83045, the value of the surface roughness parameter z_0 was estimated to be 0.25 m [9.8 in], which is indicative of sparse suburban terrain e.g. [14].

The intensity of turbulence values I_u were fitted by a Normal distribution as shown in Figure 6 for the rooftop and the panel, respectively. The rooftop values ranged from 0.27 to 0.45, with a mean of 0.30 and a coefficient of variation COV of 0.07. For the panel data, the mean value of I_u is 0.39 with a COV of 0.05. The range of values is slightly higher than that for the rooftop, reflecting its position in the disturbed flow region of the lower roof.

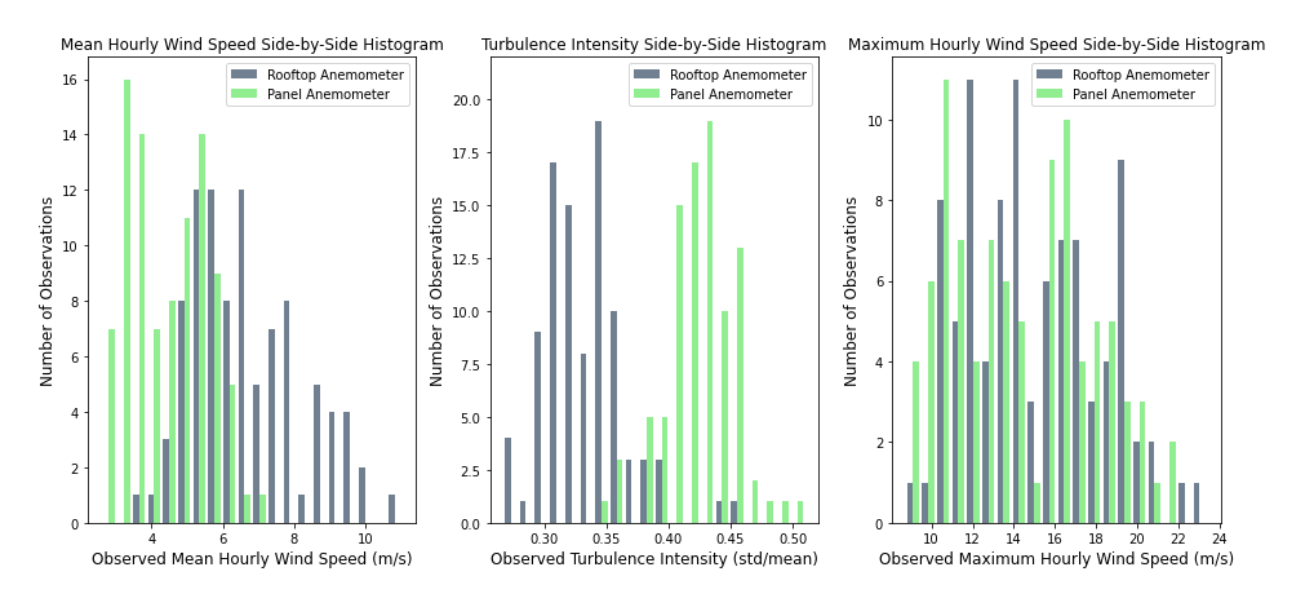


Figure 5. Histograms for the wind speed data.

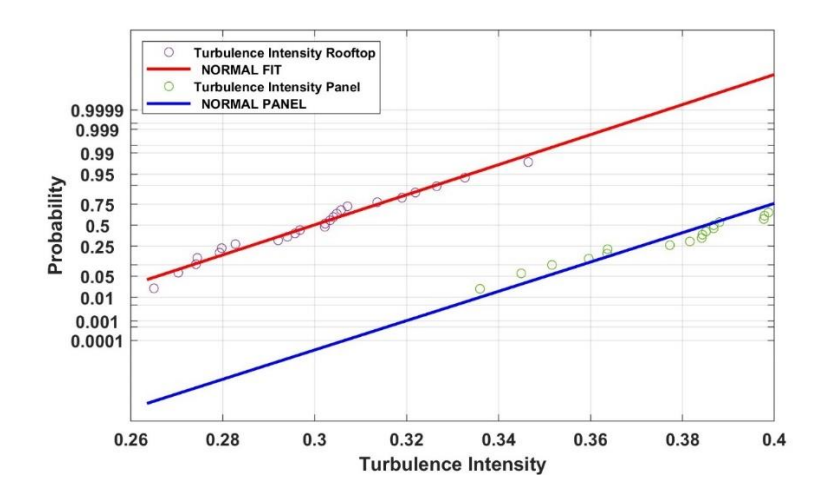


Figure 6. Normal probability plot for the turbulence intensity values for the rooftop and panel. N = 24.

The integral scales ${}^{x}L_{u}$ were derived from the integration of the autocovariance function as given in Equation 11. The rooftop data results have an approximate range of 34.6 to 81 meters for ${}^{x}L_{u}$. The mean value was 52.1 m, with a COV of 0.24. The values of the integral scales derived from the 15-minute spectra are smaller than the estimate of 106.8 m from ASCE7-22 [4]. The panel data have a smaller range of values. For the panel data, the mean ${}^{x}L_{u}$ is 9.2 m with a COV of 0.21. Both were best fitted by Normal distributions as shown in Figure 7.

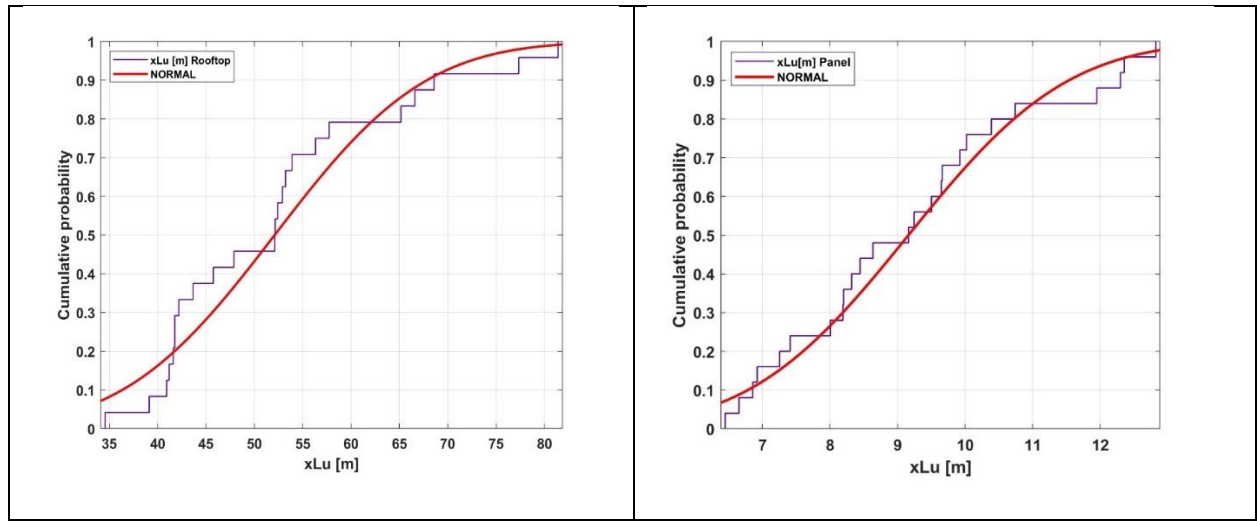


Figure 7. Integral scales of turbulence for the rooftop and panel, respectively.

3.3 Gust factor estimation and comparison with empirical methods

The data sets were used to determine the gust factor G_U is defined in Equation 2. Because the moving average and segmental approaches to time averaging provided comparable results, the segmental was employed for the records as it was computationally faster. The peak *t-second* averaged value for each hour was divided by the *mean* for that hour. The averaging time t ranged from 0.1 to 3600 seconds. These G_U are shown in Figure 8. The data exhibit a wide scatter for the smaller t values. The rooftop G_U ranged from 1.0 to 2.76 with an average of 1.57 and COV of 0.31. The panel G_U had a maximum of 3.89, with an average of 1.73, and a COV of 0.41. The best fit relationship for the rooftop data as a function of averaging time t in seconds is

228
$$\frac{U_t}{U_{3600}} = 2.059t^{-0.089}$$
 with $R^2 = 0.8539$ Equation 20

The panel data have a similar relationship as given in Equation 21:

230
$$\frac{U_t}{U_{3600}} = 2.4115t^{-0.116}$$
 with $R^2 = 0.8650$ Equation 21.

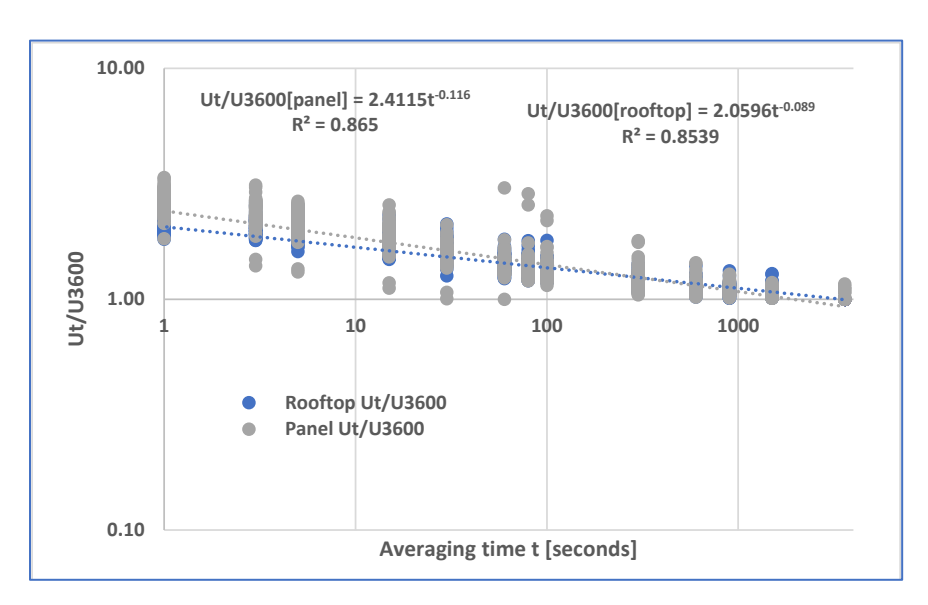


Figure 8. Gust factor plots for the rooftop and panel, respectively.

3.3.2. Comparison with empirical methods

Equation 3 was evaluated for the rooftop and panel data assuming a z_0 factor of 0.25 m [9.8 in] and the hourly mean wind speed. The results are shown in Figure 9 along with Equations 20 and 21. Also shown is the empirical approximation for the Durst curve in ASCE7-22. It can be seen that the gust factor values in the lower averaging times are underestimated by the empirical model.

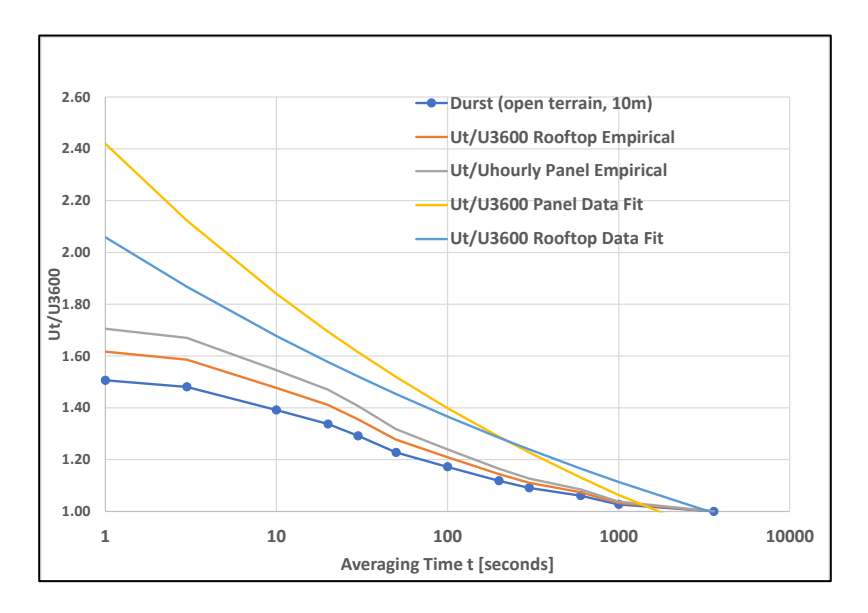


Figure 9. Comparison of data with empirical prediction method in Equation 3.

3.3.3. Extreme Value Analysis

The U_t/U_{3600} data for the lower averaging time t values display a wide scatter relative to the larger averaging times. Because the 3-second averaging time is used in ASCE7, it was evaluated for these data. Table 1 provides some sample statistics for the U_3/U_{3600} and U_3/U_{900} values for the rooftop and panel, respectively.

Table 1. Statistics for G_U for 3 seconds and 15 minutes. COV=coefficient of variation.

Statistic	Rooftop U ₃ /U ₃₆₀₀	Rooftop U ₃ /U ₉₀₀	Panel U ₃ /U ₃₆₀₀	Panel U ₃ /U ₉₀₀
Average	2.07	1.88	2.31	2.13
Maximum	2.62	2.32	2.70	2.50
Minimum	1.80	1.2	1.87	1.75
COV	0.09	0.10	0.08	0.08

Because the gust factor is a peak value divided by a mean value, the CWU measurements provide suitable data for fitting an extreme value distribution. The generalized extreme value (GEV) distribution in MATLAB [21] given in Equation 19 was found to be the best fit for U_3/U_{900} and U_3/U_{3600} as shown in Figure 10, for the rooftop and panel, respectively.

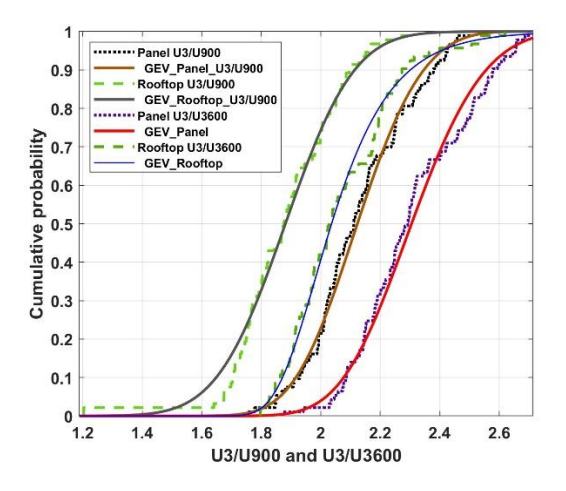


Figure 10. Gust factor distribution fitting. GEV=Generalized Extreme Value. N=94 observations.

Table 2 provides the distribution parameters for both the hourly and 15-minute (900 second) G_U values, which are commonly employed in practice.

Table 2. Generalized Extreme Value (GEV) parameters for gust factors from Equation 19.

U_3/U_{3600}	Panel GEV	Rooftop GEV	U_3/U_{900}	Panel GEV	Rooftop GEV
Mean	2.31	2.07	Mean	2.13	1.88
Variance	0.03	0.03	Variance	0.03	0.03
μ	2.24	1.99	μ	2.07	1.82
σ	0.18	0.14	σ	0.16	0.19
k	-0.23	0.013	k	-0.24	-0.36

Other G_U comparisons were made using ESDU 83045 [7]. Equation 4 for the panel data yielded a fitted g of 2.34 for the hourly data. Equations 5-9 were used to estimate relationships for the peak factor g for both the U_t/U_{900} and U_t/U_{3600} data, respectively as shown in Figure 11. Equations 22-25 were fit to the results. These peak factor values are slightly larger than those determined from the data.

Peak factor g[rooftop U_t/U_{3600}] = 3.4701 $t^{-0.117}$, $R^2 = 0.6997$. Equation 22

Peak factor g[rooftop U_t/U_{000}]=3.1323 $t^{-0.123}$, $R^2 = 0.695$.

Peak factor g[panel U_t/U_{3600}]=3.534 $t^{-0.141}$, $R^2 = 0.8322$. Equation 24

Peak factor g[panel U_t/U_{900}]=3.2056 $t^{-0.15}$, $R^2 = 0.8446$. Equation 25

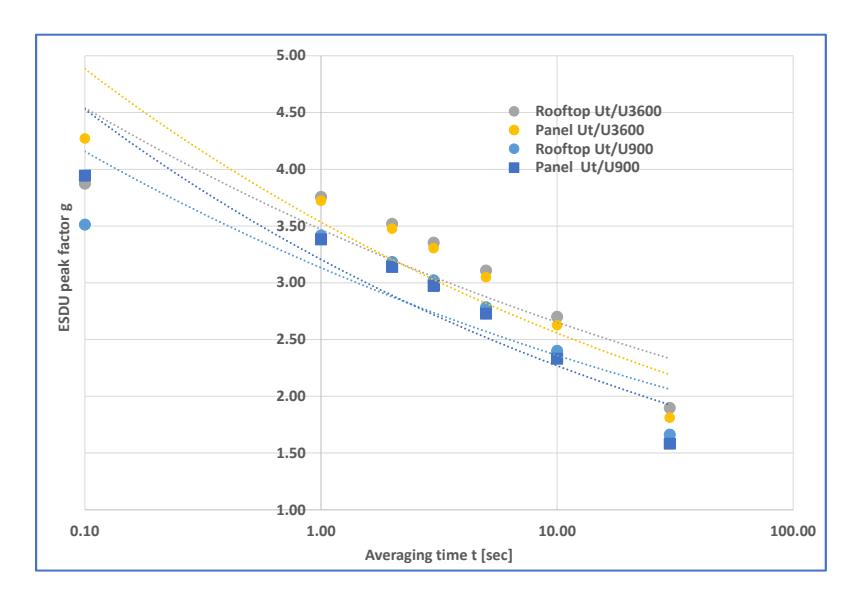


Figure 11. ESDU 83045 data fits for the peak factor g.

The method attributed to Davenport and Solari (D-S) e.g. [19, 20] as shown in Equations 13-18 was investigated for the rooftop and panel data. For this method, the rooftop mean G_U was 1.79 with associated mean $g_u = 3.01$, which matches the ESDU estimate. The mean values of the other parameters were $P_0 = 0.77$; $P_1 = 0.07$; $I_u = 0.30$; and wind speed $\overline{U} = 10$ m/s. These G_U values were close to the mean U_3/U_{3600} of 1.74 for the in situ records. The panel data resulted in D-S values of mean $G_U = 1.87$ with mean $g_u = 3.16$, which is higher than the mean $G_U = 2.10$ from the data. The mean values of the other parameters were $P_0 = 0.51$; $P_1 = 0.01$; $I_u = 0.39$; and wind speed $\overline{U} = 6.3$ m/s.

4. Results and discussion

Analysis of the spectral content for both data sets identified differences in the low and high frequency ranges. The Kaimal spectrum was a good fit to the rooftop spectrum overall, although

the rapid drop off in the higher frequency range for the data was unexpected. The slope in the higher frequency region for the rooftop data is -1.8 as opposed to -1.5. This finding should be investigated further. The spectral content for the panel anemometer located in a disturbed flow region displayed energy contributions for both low and high frequency regions. This spectrum is not representative of the Kaimal expression and illustrates the discrepancies that can occur in situ. The corresponding lower integral scale of turbulence values indicate that lower spatial correlation exists in the disturbed flow region. The large turbulence intensities for the panel also reflect the disturbed wind flow in that section of the roof. The turbulence intensity and integral scales of turbulence parameters were found to be Normal variables, with COV values of about 20%. This level of uncertainty seems reasonable for in situ conditions.

Gust factors for the rooftop and panel locations had similar trends over all averaging times, with both locations displaying a large scatter for lower *t* values. The measured sparse suburban values were larger than those for open terrain as expected. Generalized extreme value distributions provided good fits for both anemometers and simplified the process of determining extreme values for the sparse suburban conditions for given probability levels.

The entire formulation of the ASCE7 gust response factor calculations, even for rigid buildings, depends upon the gust factor G_U , the wind spectrum $S_u(n)$, and the integral scale of turbulence ${}^{x}L_u$. It has been noted that the COV for gust factors in the lower averaging times is about 30%, which suggests that the suggested gust response factor of 0.85 for rigid buildings may not be as conservative as assumed.

Finally, it is noted that the wind spectrum in situ is an important consideration in the use of the partial turbulence simulation (PTS) method employed in wind tunnel testing. FIU will explore use of the present results in the evaluation of net panel pressures e.g., [22, 23].

5. Conclusions

301

302

303

304

305

306

307

308

309

310

311

Wind speed field measurements from two ultrasonic anemometers mounted on a low-rise building in a sparse suburban terrain were presented and discussed. The Kaimal spectrum was a good fit to the rooftop data overall, with a more rapid drop off in the higher frequency range than expected. The panel spectra exhibited energy over a larger range of frequencies, which is indicative of the disturbed flow region. It was found that the gust factors display a wide scatter for low t values when plotted against the averaging time t. A generalized extreme value distribution was fit to the U_3/U_{3600} and U_3/U_{900} ratios for both anemometers. The integral scale of turbulence and the turbulence intensity were best fit by Normal distributions. The corresponding ASCE7-22 integral scale value was much higher than the field data, suggesting greater correlation than in situ.

312 Acknowledgements

- The writers acknowledge the National Science Foundation (NSF) for collaborative research awards 1824995 and 1825908 to FIU, and CWU and UW. The views and opinions expressed in
- this paper are those of the writers and do not necessarily reflect the position of the NSF.

316 References

- 317 1. Bender, W., et al., *In situ measurement of wind pressure loadings on pedestal style rooftop photovoltaic panels.* Engineering Structures, 2018. **163**: p. 281-293.
- Estephan, J. and others, Peak wind effects on low-rise building roofs and rooftop PV
 arrays, in 6th American Association for Wind Engineering Workshop, N. Kaye, Editor.
 Clemson University (online).
- 322 3. Durst, C.S., *Wind Speeds Over Short Periods of Time*. The Meteorological Magazine, 1960. **89**(1056): p. 181-186.
- Engineers, A.S.o.C., Minimum Design Loads and Associated Criteria for Buildings and
 Other Structures. 2022, ASCE.
- Wieringa, J., Gust Factors Over Open Water and Built-Up Country. Boundary Layer
 Meteorology, 1973. 3: p. 424-441.
- Greenway, M.E., *An analytical approach to wind velocity gust factors.* JWEIA, 1979. **5**: p. 61-91.

- 7. Panel, E.W.E., *Strong Winds in the Atmospheric Boundary Layer 83045*. 1983, Engineering Sciences Data Unit. p. 30.
- 332 8. Ashcroft, J., *The relationship between the gust ratio, terrain roughness, and the hourly wind speed.* JWEIA, 1994. **53**: p. 331-355.
- Krayer, W.R. and R.D. Marshall, *Gust Factors Applied to Hurricane Winds*. Bulletin
 American Meteorological Society, 1992: p. 613-617.
- 336 10. Schroeder, J.L. and D.A. Smith, *Hurricane Bonnie wind flow characteristics as* 337 *determined from WEMITE*. Journal of Wind Engineering and Industrial Aerodynamics,
 338 2003. 91: p. 767-789.
- Masters, F.J., Measurement, Modeling and Simulation of Ground-Level Tropical Cyclone
 Winds. 2004, University of Florida.
- 341 12. Yu, B. and A.G. Chowdhury, *Gust Factors and Turbulence Intensities for the Tropical*342 *Cyclone Environment.* Journal of Applied Meteorology and Climatology, 2009. **48**(3): p.
 343 534-552.
- Simiu, E., Design of Buildings for Wind: A Guide for ASCE7-10 Standard Users and
 Designers of Special Structures. Second ed. 2011, Hoboken, New Jersey: John Wiley and
 Sons. 338.
- 347 14. Simiu, E. and R.H. Scanlan, *Wind effects on structures*. 1996, NY,NY: John Wiley & Sons.
- Liu, Y., G.A. Kopp, and S.-f. Chen, An Examination of the Gust Effect Factor for Rigid
 High-Rise Buildings. Frontiers in Built Environment, 2021. 6(February).
- 351 16. ESDU, Characteristics of Atmospheric Turbulence near the Ground Part 1 ESDU,
- Editor. 1974, Engineering Sciences Data Unit Ltd.: Hartford House, 7-9 Charlotte St., London, UK.
- ESDU, Characteristics of Atmospheric Turbulence near the Ground Part II, ESDU,
 Editor. 1974, Engineering Sciences Data Unit Ltd.: London, UK.
- Davenport, A.G. and W.A. Dalgliesh, A preliminary apparaisal of wind loading concepts
 of the 1970 National Building Code of Canada, in Third International Conference on
 Wind Effects on Buildings and Structures. 1971: Tokyo, Japan.
- 359 19. Solari, G., Gust Buffeting 1: Peak wind velocity and equivalent pressure. J. Struct. Engr., 1993. 119(2): p. 365-382.
- 361 20. Solari, G., *Gust buffetting II: Dynamic alongwind reponse.* J. Struct. Engr., 1993. **119**(2): p. 383-398.
- 363 21. *MATLAB programming language*. 2020.

- Mooneghi, M.A., P. Irwin, and A.G. Chowdhury, *Partial turbulence simulation method*for predicting peak wind loads on small structures and building appurtenances. JWEIA,
 2016. **157**: p. 47-62.
- Estephan, J., A.G. Chowdhury, and P. Irwin, *A new experimental-numerical approach to estimate peak wind loads on roof-mounted photovoltaic systems by incorporating inflow turbulence and dynamic effects.* Engineering Structures, 2022. **252**.